

Simulations of turbulent transport with kinetic electrons and electromagnetic effects

Y. Chen¹, S.E. Parker¹, B.I. Cohen², A.M. Dimits², W.M. Nevins²,
D. Shumaker², V.K. Decyk³ and J.N. Leboeuf³

¹ University of Colorado, Boulder, CO, USA

² Lawrence Livermore National Laboratory, Livermore, CA, USA

³ University of California, Los Angeles, CA, USA

E-mail: yang.chen@colorado.edu

Received 8 November 2002, accepted for publication 22 August 2003

Published 12 September 2003

Online at stacks.iop.org/NF/43/1121

Abstract

A new electromagnetic kinetic electron simulation model that uses a generalized split-weight scheme, where the adiabatic part is adjustable, along with a parallel canonical momentum formulation has been developed in three-dimensional toroidal flux-tube geometry. This model includes electron–ion collisional effects and has been linearly benchmarked. It is found that for H-mode parameters, the nonadiabatic effects of kinetic electrons increase linear growth rates of the ion-temperature-gradient-driven (ITG) modes, mainly due to trapped-electron drive. The ion heat transport is also increased from that obtained with adiabatic electrons. The linear behaviour of the zonal flow is not significantly affected by kinetic electrons. The ion heat transport decreases to below the adiabatic electron level when finite plasma β is included due to finite- β stabilization of the ITG modes. This work is being carried out using the ‘Summit Framework’.

PACS numbers: 52.35.Ra, 52.65.-y

1. Introduction

Kinetic electron physics is currently a primary challenge in the simulation of magnetic fusion turbulence and transport. Until recently, the vast majority of three-dimensional gyrokinetic particle simulations with realistic geometry have used the adiabatic electron approximation [1–4]. The difficulty with a fully kinetic treatment of electrons in gyrokinetic particle simulations using the δf -method arises from the fact that for typical tokamak plasmas, where the electron and ion temperatures are of similar magnitude, the electrons move a factor of $\sim\sqrt{m_i/m_e}$ (m_i and m_e are the masses of the ion and the electron) faster than the ions along the magnetic field. This poses a stringent constraint on the time step, the Courant condition $k_{\parallel} v_{Te} \Delta t \leq 1$. To overcome this constraint, a new kinetic electron model that uses a generalized split-weight scheme [5], where the adiabatic part is adjustable, along with a parallel canonical momentum formulation, has been previously developed and benchmarked in simple geometry [6]. This is done in three-dimensional toroidal geometry using field-line-following coordinates [7]. The high- β problem in kinetic electron simulations with electromagnetic effects [6]

has been solved recently [8]. We have also implemented a Monte-Carlo electron–ion collisional algorithm and the code has been linearly benchmarked in toroidal geometry with the continuum codes GS2 [9] and GYRO [10]. This particle simulation method can now model the electron dynamics with a time step only one-third smaller than the time step typically used in adiabatic electron simulations. In this paper, we present representative simulation results on ion-temperature-gradient-driven (ITG) turbulence and transport using this new capability. The simulations are performed for a model plasma with H-mode parameters, the cyclone DIII-D base case [11]. Our focus here is on low- β , essentially electrostatic, simulations, and in addition, the effects of magnetic field perturbations on ITG turbulence and transport due to finite- β are also discussed.

A second kinetic electron model based on closing zero-inertia drift-fluid equations has been developed [12–14] and progress is being made simulating electromagnetic turbulence. This model is now running in a three-dimensional toroidal flux-tube geometry and benchmarking with the fully kinetic electron code is underway. This algorithm addresses the physics regime of higher plasma β , but not

so high that compressional Alfvén physics needs to be included. All the gyrokinetic simulation work reported here is being carried out jointly through a multi-institutional collaboration called the ‘Summit Framework’⁴, an open-source framework for both local and global massively parallel gyrokinetic turbulence simulations with kinetic electrons and electromagnetic perturbations.

The paper is organized as follows. In section 2 the algorithm for simulating kinetic electrons with electromagnetic perturbations is summarized. In section 3 the algorithm for the extended hybrid scheme is described and the current status on code development is reported. Simulation results for the DIII-D base case using the kinetic electron model as described in section 2 are presented in section 4. A summary is given in section 5.

2. Kinetic electron model

Three analytical/numerical techniques are used to make possible the direct simulation of kinetic electrons in three-dimensional geometry with electromagnetic perturbations. First, a canonical parallel momentum formulation [15] is used to eliminate numerical instabilities associated with finite-differencing of the $\partial A_{\parallel}/\partial t$ term in the parallel electric field, $E_{\parallel} = -\nabla_{\parallel}\phi - \partial A_{\parallel}/\partial t$. Second, a split-weight method [5, 6] is used for the electrons that permits larger timesteps. Third, careful numerical evaluation of the $(\omega_{pe}^2/c^2)A_{\parallel}$ term that appears in Ampere’s law in the canonical parallel momentum formulation (described in more detail below) permits accurate electromagnetic simulations at moderate β .

We begin by briefly describing the canonical momentum formulation where $p_{\parallel\alpha} = v_{\parallel\alpha} + (q_{\alpha}/m_{\alpha})(A_{\parallel})$ is used as a coordinate. The gyrokinetic equation is then

$$\frac{\partial f_{\alpha}}{\partial t} + \mathbf{v}_{G\alpha} \cdot \nabla f_{\alpha} + \dot{p}_{\parallel\alpha} \frac{\partial f_{\alpha}}{\partial p_{\parallel\alpha}} = C(f_{\alpha}), \quad (1)$$

where $\alpha = i, e$,

$$\begin{aligned} \dot{p}_{\parallel\alpha} = & \frac{q_{\alpha}}{m_{\alpha}} \tilde{\mathbf{b}} \cdot \nabla \langle \phi \rangle - \frac{\mu_{\alpha}}{m_{\alpha}} \tilde{\mathbf{b}} \cdot \nabla B + v_{\parallel\alpha} (\mathbf{b} \cdot \nabla \mathbf{b}) \cdot \mathbf{v}_E \\ & + \frac{q_{\alpha}}{m_{\alpha}} \mathbf{v}_{G\alpha} \cdot \nabla \langle A_{\parallel} \rangle \end{aligned} \quad (2)$$

and $\mathbf{v}_{G\alpha} = v_{\parallel\alpha} \tilde{\mathbf{b}} + \mathbf{v}_{d\alpha} + \mathbf{v}_E$ is the guiding centre velocity. $\tilde{\mathbf{b}} = \mathbf{b} + \langle \delta \mathbf{B}_{\perp} \rangle / B$, $\mathbf{v}_{d\alpha} = ((v_{\parallel}^2 + v_{\perp}^2)/2)/\Omega_{\alpha} B^2 \mathbf{B} \times \nabla B$ is the drift velocity for low β tokamak plasmas with $\beta \ll 1$, $\mathbf{v}_E = \langle \mathbf{E} \rangle \times \mathbf{b} / B$. Here Ω_{α} is the gyrofrequency. The electrons are described by the drift-kinetic equations due to their small gyroradii, hence $\langle \phi \rangle = \phi$, etc, for electrons. $C(f_{\alpha})$ is a collision operator. We do not consider collision effects on ions, $C(f_i) = 0$, and use a Lorentzian operator for electrons, $C(f_e) = C_L(f_e)$:

$$C_L(f_e) = v_e \frac{1}{2} \frac{\partial}{\partial \lambda} (1 - \lambda^2) \frac{\partial}{\partial \lambda} f_e, \quad (3)$$

$$v_e = \frac{n_{0e} e^4 \ln \Lambda}{4\pi \epsilon_0^2 m_e^2 v^3} \left(Z_{\text{eff}} + H_{ee} \left(\sqrt{\frac{m_e v^2}{2T_{0e}}} \right) \right) \quad (4)$$

with $H_{ee}(x) = e^{-x^2}/\sqrt{\pi}x + (1 - 1/2x^2) \text{erf}(x)$. Here, $\lambda = v_{\parallel}/v$ is the pitch-angle variable.

The ions are simulated using the usual δf method. We define $f_i = f_{0i} + \delta f_i$ with $f_{0\alpha}$ the Maxwellian distribution in $p_{\parallel\alpha}$ ($\epsilon_{\alpha} = m_{\alpha}(v_{\perp\alpha}^2 + p_{\parallel\alpha}^2)/2$),

$$f_{0\alpha} = \frac{n_{0\alpha}}{(2\pi)^{3/2} v_{T\alpha}^3} e^{-\epsilon_{\alpha}/T_{\alpha}}, \quad (5)$$

where $m_{\alpha} v_{T\alpha}^2 = T_{0\alpha}$. δf_i evolves according to

$$\frac{d\delta f_i}{dt} = - \left(v_{\parallel i} \frac{\delta B_{\perp}}{B} + \mathbf{v}_E \right) \cdot \nabla f_{0i} - \dot{\epsilon}_i \frac{\partial f_{0i}}{\partial \epsilon_i}, \quad (6)$$

where $\dot{\epsilon}_i = \mu_i \mathbf{v}_{Gi} \cdot \nabla B + m_i p_{\parallel i} \dot{p}_{\parallel i}$.

A fraction of the adiabatic part of the electrons perturbed distribution is treated separately in the split-weight scheme. Thus, we write

$$f_e = f_{0e} - \epsilon_g e \phi \frac{\partial f_{0e}}{\partial \epsilon_e} + h. \quad (7)$$

Here, ϵ_g is the split-weight parameter in the generalized split-weight scheme [6]. Typically, we choose $\epsilon_g = 0.5$. The distribution h evolves according to

$$\begin{aligned} \frac{dh}{dt} - C_L(f_e) = & - \left(v_{\parallel e} \frac{\delta B_{\perp}}{B} + \mathbf{v}_E \right) \cdot \nabla f_{0e} - \dot{\epsilon}_e \frac{\partial f_{0e}}{\partial \epsilon_e} \\ & + \epsilon_g e \left(\frac{\partial \phi}{\partial t} + \mathbf{v}_{Ge} \cdot \nabla \phi \right) \frac{\partial f_{0e}}{\partial \epsilon_e}. \end{aligned} \quad (8)$$

A Monte-Carlo scheme for the collision operator $C_L(f_e)$ is described in section 4.

The electric potential ϕ and its derivative $\dot{\phi} = \partial \phi / \partial t$ are computed from the gyrokinetic Poisson equation [16],

$$\begin{aligned} n_{0i} \frac{q_i^2}{T_{0i}} (\phi - \tilde{\phi}) + \epsilon_g n_{0e} \frac{e^2}{T_{0e}} \phi \\ = q_i \int \delta f_i \delta(\mathbf{R} + \boldsymbol{\rho} - \mathbf{x}) d\mathbf{R} d\mathbf{v} - e \int h d\mathbf{v} \end{aligned} \quad (9)$$

and its derivative

$$\begin{aligned} n_{0i} \frac{q_i^2}{T_{0i}} (\dot{\phi} - \dot{\tilde{\phi}}) = -\nabla \cdot \int q_i f_i \mathbf{v}_{Gi} \delta(\mathbf{R} + \boldsymbol{\rho} - \mathbf{x}) d\mathbf{R} d\mathbf{v} \\ + \nabla \cdot \int e f_e \mathbf{v}_{Ge} d\mathbf{v}, \end{aligned} \quad (10)$$

respectively. In equations (9) and (10), $\boldsymbol{\rho}$ is the vector leading from the gyrocentre \mathbf{R} to the particle position \mathbf{x} , $\tilde{\phi}$ is defined as

$$\tilde{\phi} = \sum_k \Gamma_0 \left(\frac{k_{\perp}^2 v_{Ti}^2}{\Omega_i^2} \right) \phi_k \exp(i\mathbf{k} \cdot \mathbf{x}) \quad (11)$$

with $\phi = \sum_k \phi_k \exp(i\mathbf{k} \cdot \mathbf{x})$. $\dot{\phi}$ and $\dot{\tilde{\phi}}$ are similarly defined.

The vector potential A_{\parallel} is given by Ampere’s law

$$\begin{aligned} \left(-\nabla_{\perp}^2 + \frac{\omega_{pe}^2}{c^2} \right) A_{\parallel} = \mu_0 \left(q_i \int \delta f_i v_{\parallel} \delta(\mathbf{R} + \boldsymbol{\rho} - \mathbf{x}) d\mathbf{R} d\mathbf{v} \right. \\ \left. - e \int h v_{\parallel} d\mathbf{v} \right). \end{aligned} \quad (12)$$

The $(\omega_{pe}^2/c^2)A_{\parallel}$ term in this equation comes from the zero-order distribution f_{0e} which is Maxwellian in p_{\parallel} . In a previous

⁴ <http://www.nersc.gov/scidac/summit>

implementation of the split-weight scheme [6] which uses equation (12) directly, it is found that at moderate β , the Alfvén wave frequency and ITG mode growth rate deviate from the linear dispersion relation significantly. This problem can be solved by evaluating the $(\omega_{pe}^2/c^2)A_{\parallel}$ term using the same marker particles and the same scattering operation as that used for the h term in equation (12), that is,

$$\frac{\omega_{pe}^2}{c^2}A_{\parallel} \approx \beta_i \frac{V}{N} \tau \sum_j p_{\parallel j}^2 A_{\parallel}(\mathbf{x}_j) S(\mathbf{x} - \mathbf{x}_j). \quad (13)$$

Here, $\tau = T_{0i}/T_{0e}$, N is the number of electrons used in the simulation, and V is the volume of the simulation box. $\beta_i = \mu_0 n_0 T_{0i}/B_0^2$ is related to the total plasma β through $\beta = 2(1 + 1/\tau)\beta_i$. $S(\mathbf{x})$ is the particle shape function used to deposit particle current to neighbouring grids. The resulting form of the Ampere's equation has a matrix that depends on the particle coordinates and time and is three-dimensional. The detailed algorithm has been presented elsewhere [8]. For very low β cases ($\beta_i m_i/m_e \ll 1$) that are essentially electrostatic, equation (12) is used for better computational efficiency.

3. Kinetic electron extended hybrid algorithm

A hybrid simulation scheme that includes electromagnetic effects has been previously proposed and study in a slab geometry shows that it can adequately simulate the shear Alfvén waves and the finite β effects on the ITG waves [12]. In this hybrid model, ions are treated as gyrokinetic while electrons are described by fluid equations. Recently, a kinetic electron closure valid for $\beta m_i/m_e \geq 1$ has been introduced [13, 14]. The new algorithm incorporates δf drift-kinetic electrons whose number-density moment is used to close the electron fluid momentum equation (Ohm's law). A toroidal extension of the hybrid algorithm has been formulated, and the code implementation is being validated. Two-dimensional slab test cases have examined small-amplitude kinetic shear Alfvén waves with electron Landau damping, the ion-temperature-gradient instability, and the collisionless drift instability in an unshered slab as a function of β [13]. The scheme, which is to be included as part of the Summit Framework, can be summarized as follows. The electron distribution function is given as $f_e = f_{0e} + (\delta n_e^{(0)}/n_{0e})f_{0e} + h$, where $\delta n_e^{(0)}$ is the lowest-order fluid component of the perturbed electron density. The total perturbed electron density $\delta n_e = \delta n_e^{(0)} + \delta n_e^K$ ($\delta n_e^K = \int h dv$) is obtained from the electron continuity equation deduced from the electron drift-kinetic equation. A_{\parallel} is advanced in time according to $\partial A_{\parallel}/\partial t = -\nabla_{\parallel} \phi - E_{\parallel}$. E_{\parallel} is obtained from the parallel Ohm's law which utilizes a kinetic closure for the electron pressure [17]: $\nabla_{\parallel} P_{\parallel e} = \nabla_{\parallel} P_{\parallel e}^{(0)} + T_{\parallel e}^{(0)} \nabla_{\parallel} \delta n_e^{(0)} + n_{0e} \nabla_{\parallel} \delta T_{\parallel e}$ where $\nabla_{\parallel} \equiv \mathbf{b} \cdot \nabla$. $\nabla_{\parallel} (T_{\parallel e}^{(eq)} + \delta T_{\parallel e}) = 0$ is imposed [17], $T_{\parallel e}^{(eq)}$ is the equilibrium temperature (including gradients) and $P_{\parallel e}^{(0)} = n_{0e} T_{\parallel e}^{(eq)}$. Nonadiabatic kinetic corrections to the pressure moment are higher order in $(\omega/k_{\parallel} v_{Te})^2$ than are the terms coming from the adiabatic response [11]. With the updated A_{\parallel} , Ampere's law determines the parallel electron current (needed for evolving the electron continuity equation): $en_{0e} u_{\parallel e} = (1/\mu_0) \nabla_{\perp}^2 A_{\parallel} + \delta j_{\parallel i}$, where $\delta j_{\parallel i}$ is the perturbed parallel ion current. The electrostatic

potential is obtained from the quasi-neutrality condition using the updated total electron and ion charge densities. Once A_{\parallel} and ϕ are available, ion and electron coordinates and weights are evolved according to the ion gyrokinetic equation and the electron drift kinetic equation written in terms of h .

With electron inertia retained in the extended hybrid algorithm, the scheme is numerically unstable for $\beta_i m_i/m_e < 1$, because the Alfvén velocity then exceeds the electron thermal velocity and the electron response is therefore not adiabatic. For $k_{\perp} \rho_i > 1$, the value of β_i below which the extended hybrid algorithm is badly behaved increases. However, when the electron inertia is neglected in the electron fluid momentum balance (valid if the fluid response is dominantly adiabatic), the value of β_i below which the extended hybrid algorithm is badly behaved decreases substantially. The kinetic extended hybrid scheme remains useful over an interestingly large range of β_i for including kinetic electron corrections when the electrons as a whole are dominantly adiabatic.

In sheared-slab configurations, the electron response transitions from hydrodynamic to resonant and lastly to adiabatic as a function of distance from the mode rational surface where $k_{\parallel} = 0$. Because the formal expansion of the kinetic extended electron hybrid equations is around an adiabatic fluid response like the expansion in Lin and Chen [18], this treatment is invalid in the resonance layer near the mode rational surface. When trying to simulate the ion-temperature-gradient instability in a sheared slab using the hybrid algorithm, we observed enhanced Alfvénic noise and growing modes (that saturated), but not easily identifiable ITG signal. In a torus, the mode structure along the field line is finite in extent, and it is argued that the slab branch is not as important as the toroidal branch in driving transport because the radial scales of the slab branch are narrow. It remains to be investigated whether the hybrid algorithm is practical in toroidal configurations, and this effort is in progress.

4. Simulation results with kinetic electrons

In this section, we present linear and nonlinear simulation results for a representative tokamak plasma, the DIII-D cyclone base case [11]. We first summarize the geometry and computational method as follows. An equilibrium with concentric flux surfaces is assumed. The magnetic field strength is $B(r, \theta) = B_0(1 - (r/R_0) \cos \theta)$. The field-line-following coordinates [7] (x, y, z) are defined by $x = r - r_0$, $y = (r_0/q_0)(q\theta - \zeta)$, and $z = q_0 R_0 \theta$. Here, (r, θ, ζ) are the usual toroidal coordinates, R_0 is the major radius at the magnetic axis, r_0 is the minor radius at the centre of the simulation domain, $q_0 = q(r_0)$ the safety factor. The size of the simulation box along the field line is $2\pi q_0 R_0$. Periodic boundary conditions are used in x and y , while the toroidal boundary condition [7] is used in z . By assuming periodicity in radius at fixed y , relaxation of the background equilibrium temperature and density profiles is prevented, even if no particle and heat sources are used. However, spatially localized perturbations of the temperature and density profiles do occur. A predictor–corrector scheme is used to advance particle coordinates and weights. The field equations (9), (10) and (12) are solved spectrally [6]. The Lorentz operator $C_L(f_e)$

is implemented as follows. From equation (7)

$$C_L(f_e) = C_L(f_{0e}(p_{\parallel})) - C_L\left(\epsilon_g \phi \frac{\partial f_{0e}}{\partial \epsilon_e}\right) + C_L(h). \quad (14)$$

The ϵ_g term is nonlinear and will be neglected. The first term is given by

$$C_L(f_{0e}(p_{\parallel})) = -\tau v_e A_{\parallel} f_{0e}, \quad (15)$$

which is implemented as an additional term in the electron weight equation. The third term on the right-hand side of equation (14) is implemented using a Monte-Carlo method [19,20],

$$\lambda_{\text{new}} = \lambda_{\text{old}}(1 - v_e \delta t) \pm [(1 - \lambda_{\text{old}}^2) v_e \delta t]^{1/2}, \quad (16)$$

where \pm means equal probability of + or - [19]. $\delta t = \Delta t$ for the corrector step and $\delta t = 2\Delta t$ for the predictor step, Δt is the time step of the simulation.

In the following simulations, we use the DIII-D base-case parameters: the equilibrium gradient scale lengths are $R_0/L_n = 2.2$, $R_0/L_{Ti} = 6.9$, $R_0/L_{Te} = 0$, $T_{0i} = T_{0e}$, $r_0/R_0 = 0.18$, $q_0 = 1.4$, and $\hat{s} = (r_0/q_0)(dq/dr) = 0.78$. Most of the simulation results are obtained with $\beta = 4 \times 10^{-4}$. This small β is not important physically, and the simulations are essentially electrostatic. However, the small but nonzero β allows an increased time step, possibly because the high frequency ω_H mode [21] is avoided. In all the simulations with kinetic electrons, the mass ratio is $m_i/m_e = 1837$, and the split-weight parameter is $\epsilon_g = 0.5$. Figure 1 shows the growth rate and frequency of the $k_{\theta}\rho_i = 0.3$ mode as a function of R_0/L_T for $v_{ei} = 0$. Also shown are the results from the GS2 code with kinetic electrons. Very good agreement is seen between GS2 results and those from the split-weight particle code. For the base case $R_0/L_{Ti} = 6.9$, the linear growth rate with kinetic electrons is $\gamma L_n/v_{Ti} = 0.21$. The result obtained from simulations with adiabatic electrons is $\gamma L_n/v_{Ti} = 0.12$. In the kinetic electron simulation, we can treat the passing electrons as adiabatic and follow only the trapped electrons. The growth rate thus obtained is very close to the kinetic

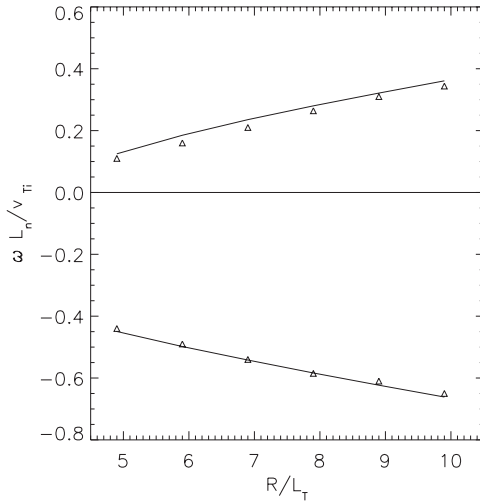


Figure 1. Growth rate and frequency of the $k_{\theta}\rho_i = 0.3$ mode versus R/L_T , comparing the split-weight particle code with GS2. Upper part is for growth rates. Data points are from particle simulations.

electron result, hence the increase of the growth rate from the adiabatic electron result is mainly due to the nonadiabatic effect of the trapped electrons. Figure 2 shows the mode growth rate as a function of $k_{\theta}\rho_i$ for the base case with $v_{ei}L_n/v_{Ti} = 0.136$. Results from both kinetic electrons and adiabatic electrons are shown. The results are obtained from linear simulations in which only a single k_{θ} mode is retained.

Figure 3 shows the evolution of the ion heat diffusivity χ_i (ion heat flux $\langle \int d\mathbf{v} \hat{r} \cdot \mathbf{v} E \frac{1}{2} m_i v^2 \delta f_i \rangle$ normalized by $1/L_{Ti}$) with $R/L_{Ti} = 6.9$, for two cases: (a) with kinetic electrons, $\beta = 4 \times 10^{-4}$ and $v_{ei}L_n/v_{Ti} = 0.45$; (b) with adiabatic electrons. The case (a) result is obtained with a simulation box of $l_x = l_y = 128\rho_i$ resolved by 128×128 grids in the x - y plane. The number of grid points in the z direction is 32. A total of 16 777 216 particles per species is loaded, and a time step of $\Delta t \omega_{ci} = 4$ is used. As can be seen

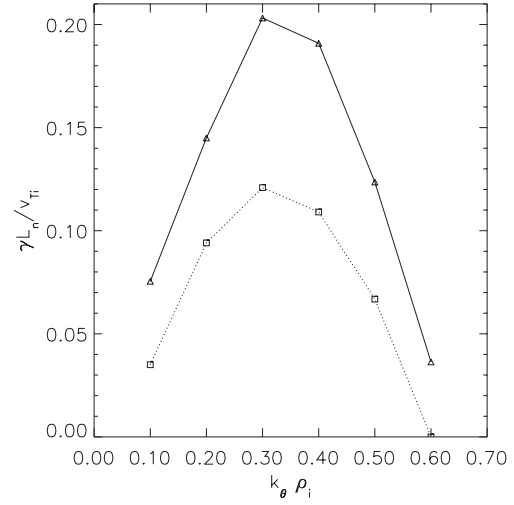


Figure 2. ITG mode growth rate versus k_{θ} . Upper curve from kinetic electron simulations, lower curve from adiabatic electron simulations.

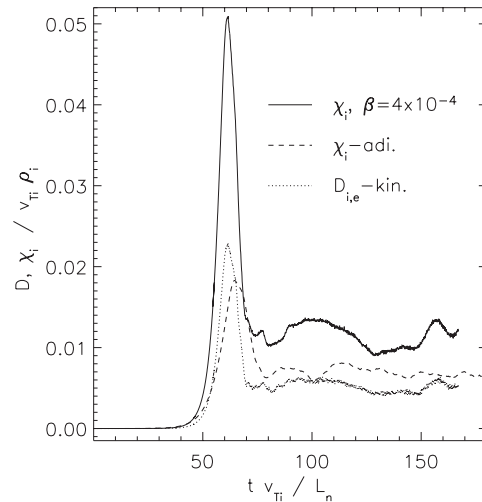


Figure 3. Evolution of the ion heat flux and particle diffusivity for the base case parameters.

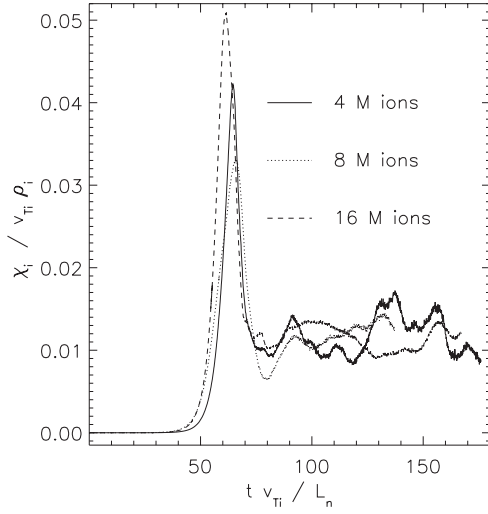


Figure 4. Convergence test with respect to particle number and box size.

from (a) and (b), with kinetic electrons the ion heat diffusivity is about $\chi_i/\rho_i v_{Ti} = 0.01$, significantly increased from that with adiabatic electrons, $\chi_i/\rho_i v_{Ti} = 0.0065$. This is roughly consistent with the increase in linear growth rates (see figure 2). As a result of the nonadiabatic effect of the electrons, a finite particle number flux is observed in the simulation corresponding to case (a), which is also shown in figure 3 (normalized by $1/L_{Ti}$). The turbulent particle transport is intrinsically ambipolar (consistent with the assumption and use of the quasi-neutrality relation), with a diffusivity of about $D_i/\rho_i v_{Ti} \approx 0.016$.

The nonlinear result with kinetic electrons in case (a) of figure 3 is converged with respect to the size of the simulation box and particle numbers. Figure 4 shows the results of this convergence test. The cases shown are: (i) box size $l_x \times l_y = 64\rho_i \times 64\rho_i$, 4 194 304 particles per species; (ii) $l_x \times l_y = 128\rho_i \times 128\rho_i$, 8 388 608 particles per species; and (iii) $l_x \times l_y = 128\rho_i \times 128\rho_i$, 16 777 216 particles per species corresponding to case (a) in figure 3. Grid sizes are $\Delta x = \Delta y = \rho_i$, $\Delta z = l_z/32$. Time step $\omega_{ci}\Delta t = 4$, $v_{ei}/\omega_{ci} = 10^{-3}$. One can see that convergence with respect to box size and particle number is achieved with a box size of $64\rho_i \times 64\rho_i$ and 32 particles per grid cell.

Since the turbulence-generated zonal flow plays an important role in regulating turbulence and transport [22], it is of interest to study the effects of kinetic electrons on the evolution of the geodesic acoustic mode (GAM) and the residual zonal flow [23, 24]. Theory predicts no significant change due to kinetic electron effects. Figure 5 shows the evolution of the GAM with kinetic electrons (the solid line) and adiabatic electrons (the dashed line). A scan of the residual zonal flow level with changing q is shown in figure 6, where the residual zonal flow level $\phi(\infty)/\phi(0)$ is plotted as a function of $h = \sqrt{\varepsilon}/q^2$ ($\varepsilon = r_0/R_0$). The line is predicted by the Rosenbluth–Hinton theory [23, 24] assuming adiabatic electrons. The simulation is initialized with a perturbed ion density while the perturbed electron density is set to zero. Only the $k_\theta = 0$ mode is retained and the simulation is linear. As

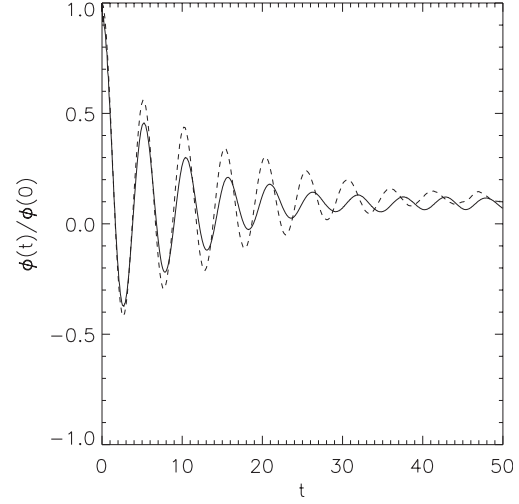


Figure 5. Evolution of the GAM and the residual zonal flow. Dashed line is obtained with adiabatic electrons, solid line with kinetic electrons.

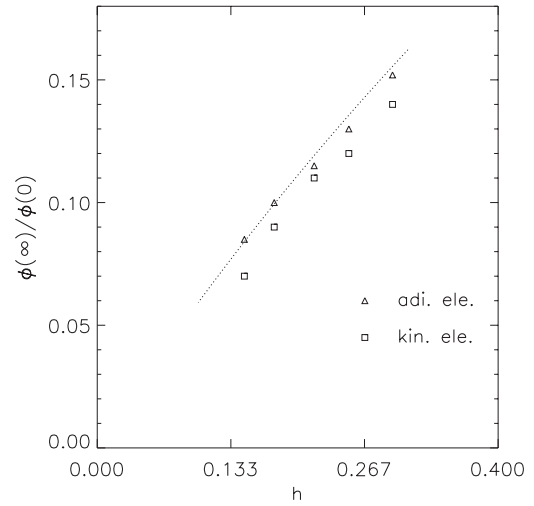


Figure 6. The residual level of the zonal flow versus magnetic shear. The line is predicted by the Rosenbluth–Hinton theory.

can be seen from figures 5 and 6 the residual level of the zonal flow is not significantly changed by kinetic electrons. This is consistent with the nonlinear results in figure 3, which shows an increase of the saturated ion heat flux that can be understood based on linear physics.

We now discuss the finite- β effects on the ITG turbulence and transport. The time-averaged ion heat diffusivity χ_i (normalized by $v_{Ti}\rho_i^2/L_n$) is plotted versus β in figure 7, as well as the growth rate of the $k_\theta\rho_i = 0.3$ mode. The perpendicular box size is $65.3\rho_i \times 64\rho_i$, and the grid number is 64×64 . The number of particles per species is 4 194 304, and the time step is $\omega_{ci}\Delta t = 3$. Other parameters are $v_{ei}L_n/v_{Ti} = 0.136$, $m_i/m_e = 1837$, $\varepsilon_g = 0.5$. For the following simulations, equation (13) is used, since $\beta m_i/m_e \gg k_\perp^2\rho_i^2$. The adiabatic electron result in figure 3(a) corresponds to $\chi_i/\rho_i v_{Ti} \approx 2.9$. As β is increased from zero, the ITG modes becomes less unstable due to finite- β stabilization, and the saturated ion

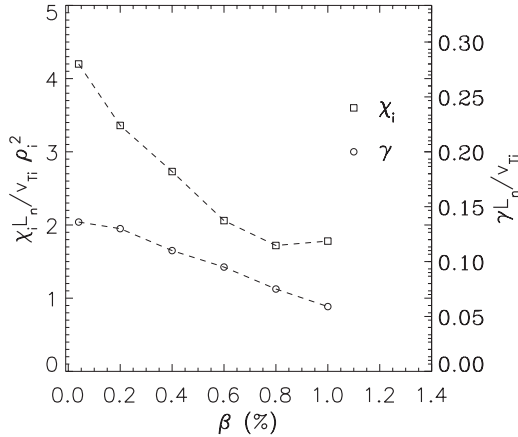


Figure 7. Ion heat diffusivity and the growth rate of the $k_\theta \rho_i = 0.3$ mode versus β , for $\eta_e = 0$, showing the finite β stabilization of the ITG mode.

heat flux is also reduced to below the adiabatic electron level. These results are obtained with $\eta_e = 0$ ($\eta_e = L_n/L_{Te}$). We have also carried out simulations with $\eta_e = \eta_i$, which show the same trend of finite- β stabilization and reduction to the ion heat flux as in the $\eta_e = 0$ case. Over the same range of β , the dominant mode, $k_\theta \rho_i = 0.3$, is more unstable for $\eta_e = \eta_i$ than for the case of $\eta_e = 0$, and the saturated ion heat diffusivity is also higher. For $\beta = 0.8\%$, the ion heat diffusivity is $\chi_i/\rho_i \nu_{Ti} \approx 4$ for $\eta_e = \eta_i$, compared with $\chi_i/\rho_i \nu_{Ti} \approx 1.7$ for $\eta_e = 0$. These dominant instabilities have frequencies very close to the frequencies at zero β , hence are determined to be the finite- β modified ITG modes. The results for the finite- β ITG branch that growth rates and thermal diffusivities decrease with increasing β are consistent with the simulation results obtained with a fluid electron model in [25]. We have also attempted to extend the nonlinear simulations to β regimes where the kinetic ballooning modes are dominant. However, at present these simulations are a more difficult undertaking due to the following reasons: (a) at high β the radial profile of the unstable modes tends to develop fine structures [26], which requires finer radial grid size; (b) as β increases the spectrum of unstable modes extends to longer wavelengths, which requires a larger simulation domain; and (c) as the amplitude of the magnetic fluctuation (which is proportional to β) increases, the weights of the electrons grow more rapidly, which requires substantially more particles to reduce the statistical noise. Thus, nonlinear simulations in the KBM regime are more demanding of computer resources than are the ITG simulations. Work on the KBM regime is still in progress.

The experimentally measured ion heat diffusivity for the DIII-D shot (shot #81499 at time $t = 4000$ ms, on which the base case parameters are based) is $\chi_i = 0.16$ [11] in the unit of figure 7, much lower than the adiabatic electron level. Since we do not yet have effects such as profile variation, equilibrium shear flows, realistic geometry, impurities, etc, in the model, this discrepancy between simulation and experimental data cannot be fully resolved at the present time. Nevertheless, the simulation results presented here indicate that electromagnetic effects on the ITG turbulence could play an important role in determining the transport level.

5. Summary

In this paper, we present simulation results for the ITG turbulence and transport using the DIII-D cyclone base case parameters [11]. The simulations use a δf gyrokinetic particle method that includes fully kinetic electrons, three-dimensional toroidal geometry using field-line-following coordinates, and electromagnetic effects. Consistent with the increased linear growth rates of the ITG modes due to trapped-electron drive, the saturated ion heat transport is increased from that obtained with adiabatic electrons. The evolution of zonal flows is not significantly changed by kinetic electrons, consistent with analytical theory [23, 24]. It is shown that finite- β stabilization of the ITG modes can effectively reduce the saturated ion heat transport. The code is implemented as part of the Summit Framework. Summit is a collaborative effort aimed at both local and global massively parallel gyrokinetic turbulence simulations with kinetic electrons and electromagnetic perturbations. A hybrid model in which electrons are treated by fluid equations with kinetic electron closure is also described.

Acknowledgments

This work is part of the Summit Framework, Computational Center for the Study of Plasma Microturbulence, an Office of Fusion Energy Sciences, United States Department of Energy, Scientific Discovery through Advanced Computing (SciDAC) Project. We thank Dr W. Dorland for help with generating GS2 linear benchmarks.

References

- [1] Parker S., Lee W. and Santoro R. 1993 *Phys. Rev. Lett.* **71** 2042
- [2] Dimits A., Williams T., Byers J. and Cohen B. 1996 *Phys. Rev. Lett.* **77** 71
- [3] Sydora R., Decyk V. and Dawson J. 1996 *Plasma Phys. Control. Fusion* **38** A281
- [4] Lin Z., Hahn T., Lee W., Tang W. and White R. 1998 *Science* **281** 1835
- [5] Manuilskiy I. and Lee W.W. 2000 *Phys. Plasmas* **7** 1381
- [6] Chen Y. and Parker S.E. 2001 *Phys. Plasmas* **8** 2095
- [7] Beer M.A., Cowley S.C. and Hammett G.W. 1995 *Phys. Plasmas* **2** 2687
- [8] Chen Y. and Parker S. 2003 *J. Comput. Phys.* **189** 463
- [9] Dorland W., Jenko F., Kotschenreuther M. and Rogers B. 2000 *Phys. Rev. Lett.* **25** 5579
- [10] Candy J. and Waltz R. 2003 *J. Comput. Phys.* **186** 545
- [11] Dimits A. *et al* 2000 *Phys. Plasmas* **7** 969
- [12] Chen Y. and Parker S.E. 2001 *Phys. Plasmas* **8** 441
- [13] Cohen B.I., Dimits A.M., Nevins W., Chen Y. and Parker S.E. 2002 *Phys. Plasmas* **9** 251
- [14] Cohen B.I., Dimits A.M., Nevins W., Chen Y. and Parker S.E. 2002 *Phys. Plasmas* **9** 1915
- [15] Hahn T.S., Lee W.W. and Brizard A. 1988 *Phys. Fluids* **31** 1940
- [16] Lee W.W. 1983 *Phys. Fluids* **26** 556
- [17] Snyder P. 1999 *PhD Thesis* Gyrofluid Theory and simulation of electromagnetic turbulence and transport in tokamaks (New Jersey: Princeton)
- [18] Lin Z. and Chen L. 2001 *Phys. Plasmas* **8** 1447
- [19] Boozer A.H. and Kuo-Petravic G. 1981 *Phys. Fluids* **24** 851
- [20] Chen Y. and White R.B. 1997 *Phys. Plasmas* **10** 3591
- [21] Lee W. 1987 *J. Comput. Phys.* **72** 243

-
- [22] Diamond P. and Kim Y. 1991 *Phys. Fluids B* **3** 1626
- [23] Rosenbluth M.N. and Hinton F.L. 1998 *Phys. Rev. Lett.* **80** 724
- [24] Hinton F.L. and Rosenbluth M.N. 1999 *Plasma Phys. Control. Fusion* **41**
- [25] Snyder P. and Hammet G. 2001 *Phys. Plasmas* **8** 744
- [26] Falchetto G.L. 2001 Electromagnetic microinstabilities in tokamak plasmas using a global spectral approach *PhD Thesis* Center de Recherches en Physique des Plasmas, Association Euratom-Confederation Suisse, Ecole Polytechnique Federale de Lausanne, CRPP-PPB, CH-1015 Ecublens, Switzerland